J|A|C|S
ARTICLES
Published on Web 04/28/2006

Design of Functional Ferritin-Like Proteins with Hydrophobic Cavities

Joe Swift, William A. Wehbi, Brenna D. Kelly, Xiaoran Fu Stowell,[1] Jeffery G. Saven, and Ivan J. Dmochowski*

Contribution from the Department of Chemistry, University of Pennsylvania, 231 South 34th Street, Philadelphia, Pennsylvania 19104-6323

Received October 17, 2005; E-mail: ivandmo@sas.upenn.edu

Abstract: Ferritin four-helix bundle subunits self-assemble to create a stable multimer with a large central hydrophilic cavity where metal ions bind. To explore the versatility of this reaction vessel, computational design was used to generate cavities with increasingly apolar surface areas inside a dodecameric ferritin-like protein, Dps. Cavity mutants, in which as many as 120 surface accessible hydrophilic residues were replaced with hydrophobic amino acids, were shown to still assemble properly using size-exclusion chromatography and dynamic light scattering measurements. Wild-type Dps exhibited highly cooperative subunit folding and assembly, which was monitored by changes in Trp fluorescence and UV circular dichroism. The hydrophobic cavity mutants showed distinctly less cooperative unfolding behavior, with one mutant forming a partially assembled intermediate upon guanidine denaturation. Although the stability of Dps to such denaturation decreased with increasing apolar surface area, all proteins exhibited high melting temperatures, $T_m = 74-90$ °C. Despite the large number of mutations, near-native ability to mineralize iron was maintained. This work illustrates the versatility of the ferritin scaffold for engineering large protein cavities with novel properties.

Introduction

The ferritin iron storage proteins[2] serve as diverse and powerful scaffolds for the design of complex nanomolecular structures.[3,4] Twelve or 24 ferritin four-helix bundles self-assemble to give a hollow holoprotein. The outer and inner diameters are 9−12 and 4−8.5 nm, respectively, which vary with the source of the protein.[5,6] Ferritin multimers are non-covalently assembled but typically remain intact over a wide range of pH and temperature.[7] This unusually large, robust yet flexible protein architecture recommends ferritin for the design of molecular containers of varied size and function.

Beyond its role in biological iron storage, ferritin binds many other divalent metals, and its large cavity can template the synthesis of inorganic nanoparticles,[8−10] minerals,[11−14] and semiconductors.[15−17] Ferritins also have modest affinity for organic small molecules, such as the anesthetic halothane,[18] the chemotherapeutic doxorubicin,[19] and the pH indicator neutral red,[20] but these compounds have not been shown definitively to bind in the central cavity. Halothane, for example, was identified crystallographically in horse spleen ferritin only in the small hydrophobic pocket at each 2-fold symmetric subunit interface.[18] Recent studies have shown that metal nanoparticles can be synthesized and stabilized through hydrophobic interactions with cyclodextrins,[21] alkane-modified peptides,[22] and dendrimers.[23] Hence, increasing the hydrophobicity of a ferritin-like protein cavity could enhance the formation of metal nanoparticles, as well as the binding of many compounds for chemical reactions, molecular storage, and delivery.

Exploring the stability of ferritin-like cavities toward hydrophobic mutations complements widespread efforts to design cavities in other proteins.[24−29] Wong et al. previously created organic-soluble ferritins by coupling alkyl chains to surface

(1) Present address: Department of Biology, M.I.T., 77 Massachusetts Ave., Cambridge, MA 02139.
(2) Liu, X.; Theil, E. C. *Acc. Chem. Res.* **2005**, *38*, 167−175.
(3) Dickson, D. P. E.; Walton, S. A.; Mann, S.; Wong, K. *Nanostruct. Mater.* **1997**, *9*, 595−598.
(4) Hosein, H. A.; Strongin, D. R.; Allen, M.; Douglas, T. *Langmuir* **2004**, *20*, 10283−10287.
(5) Hempstead, P. D.; Yewdall, S. J.; Fernie, A. R.; Lawson, D. M.; Artymiuk, P. J.; Rice, D. W.; Ford, G. C.; Harrison, P. M. *J. Mol. Biol.* **1997**, *268*, 424−448.
(6) Johnson, E.; Cascio, D.; Sawaya, M. R.; Gingery, M.; Schroder, I. *Structure* **2005**, *13*, 637−648.
(7) Harrison, P. M.; Arosio, P. *Biochim. Biophys. Acta* **1996**, *1275*, 161−203.
(8) Dominguez-Vera, J. M.; Colacio, E. *Inorg. Chem.* **2003**, *42*, 6983−6985.
(9) Ensign, D.; Young, M.; Douglas, T. *Inorg. Chem.* **2004**, *43*, 3441−3446.
(10) Ueno, T.; Suzuki, M.; Goto, T.; Matsumoto, T.; Nagayama, K.; Watanabe, Y. *Angew. Chem., Int. Ed. Engl.* **2004**, *43*, 2527−2530.
(11) Meldrum, F. C.; Heywood, B. R.; Mann, S. *Science* **1992**, *257*, 522−523.
(12) Meldrum, F. C.; Douglas, T.; Levi, S.; Arosio, P.; Mann, S. *J. Inorg. Biochem.* **1995**, *58*, 59−68.
(13) Douglas, T.; Stark, V. T. *Inorg. Chem.* **2000**, *39*, 1828−1830.
(14) Allen, M.; Willits, D.; Young, M.; Douglas, T. *Inorg. Chem.* **2003**, *42*, 6300−6305.
(15) Douglas, T.; Dickson, D. P. E.; Betteridge, S.; Charnock, J.; Garner, C. D.; Mann, S. *Science* **1995**, *269*, 54−57.
(16) Wong, K. K. W.; Mann, S. *Adv. Mater.* **1996**, *8*, 928−932.
(17) Yamashita, I.; Hayashi, J.; Hara, M. *Chem. Lett.* **2004**, *33*, 1158−1159.
(18) Liu, R.; Loll, P. J.; Eckenhoff, R. G. *FASEB J.* **2005**, *19*, 567−576.
(19) Simsek, E.; Kilic, M. A. *J. Magn. Magn. Mater.* **2005**, *293*, 509−513.
(20) Webb, B.; Frame, J.; Zhao, Z.; Lee, M. L.; Watt, G. D. *Arch. Biochem. Biophys.* **1994**, *309*, 178−183.
(21) Liu, Y.; Male, K. B.; Bouvrette, P.; Luong, J. H. T. *Chem. Mater.* **2003**, *15*, 4172−4180.
(22) Djalali, R.; Samson, J.; Matsui, H. *J. Am. Chem. Soc.* **2004**, *126*, 7935−7939.
(23) Esumi, K.; Hosoya, T.; Suzuki, A.; Torigoe, K. *J. Colloid Interface Sci.* **2000**, *229*, 303−306.

carboxylic acid residues.[30] In contrast, the proteins described herein form structures where the interior hydrophobic surface is surrounded by the protein shell.

For this initial effort, we chose a homopolymeric ferritin-like protein, Dps (DNA binding protein from starved cells), which is the major protein expressed in bacteria under starvation conditions.[31] Members of the Dps subfamily lack the C-terminal fifth-helix of 24-mer ferritins, and assemble to form only dodecameric protein shells with 23 symmetry and outer and inner diameters of 9 and 4.5 nm.[32] Dps stores ~500 iron atoms as a ferric hydroxide mineral core,[33,34] binds and protects DNA from oxidative damage and cleavage by endonucleases,[35] and plays important roles in nucleoid compaction and protecting bacterial cells against multiple stresses during the stationary phase.[36−38] Despite the high molecular weight (~220 kD) of the homododecamer, Dps is amenable to rational computational design due to its high symmetry, as well as its stable tertiary and quaternary structures.

Many mutagenesis studies involving ferritin proteins have been performed previously.[39−41] For example, Wade et al. mutated several glutamic acid residues in the cavity of recombinant human ferritin, to examine their role in iron core formation.[40] In this paper, we similarly explored the role of some key iron-binding residues inside the Dps cavity, which is particularly interesting in light of recent crystallographic studies showing well-ordered iron atoms in Dps proteins.[34,42]

Despite recent advances in protein synthetic and computational methods,[43−53] it is still a considerable challenge to design proteins with an internal cavity, as it typically destabilizes hydrophobic packing interactions.[54,55] For example, a T4 lysozyme was destabilized by 2.7−5.0 kcal/mol upon introduction of single cavity-forming point mutations within the hydrophobic core,[29] and studies on barnase cavity mutations[25,26] found that protein stability was inversely proportional to the cavity volume. For these hydrophobic cavities, whose interior size ranged from 50 to 500 Å^3, the stability decreased upon mutation of interior residues. To create proteins with much larger (~50 000 Å^3) hydrophobic interiors, we employed computational methods to redesign the internal cavity of a naturally occurring ferritin-like protein.

Computational redesign of existing proteins has previously yielded structures with novel properties.[46,56−58] Examples include the creation of maquettes[59] that bind porphyrins[60] or metals[47] and proteins with catalytic activity.[61] Several different algorithms allow sequence searches for energy minima, including pruning and dead-end elimination,[62] Monte Carlo,[63] and simulated annealing.[57,64] Complementary to these approaches are statistical and probabilistic approaches to protein design,[48,65] which yield the site-specific likelihoods of the amino acids among sequences likely to fold to a given three-dimensional structure.[64,66−69] Recent experiments validating such a probabilisitic approach include the design of a water-soluble membrane potassium channel protein,[70] four-helix bundles that bind metals[47] or nonbiological cofactors,[60] and redox-active rubredoxin mimics.[71] This method was extended recently to include symmetric quaternary structures,[69] which facilitated the present study.

Herein, a probabilistic computational design method was used to guide the design of novel ferritin-like proteins, variants of *Escherichia coli* Dps, with hydrophobic interiors. The present study illustrates how computational design can facilitate such wide-scale mutagenesis efforts. The resulting proteins were

(24) Mooers, B. H. M.; Datta, D.; Baase, W. A.; Zollars, E. S.; Mayo, S. L.; Matthews, B. W. *J. Mol. Biol.* **2003**, *332*, 741−756.
(25) Buckle, A. M.; Cramer, P.; Fersht, A. R. *Biochemistry* **1996**, *35*, 4298−4305.
(26) Axe, D. D.; Foster, N. W.; Fersht, A. R. *Proc. Natl. Acad. Sci. U.S.A.* **1996**, *93*, 5590−5594.
(27) Jackson, S. E.; Moracci, M.; Elmasry, N.; Johnson, C. M.; Fersht, A. R. *Biochemistry* **1993**, *32*, 11259−11269.
(28) Eriksson, A. E.; Baase, W. A.; Wozniak, J. A.; Matthews, B. W. *Nature* **1992**, *355*, 371−373.
(29) Eriksson, A. E.; Baase, W. A.; Zhang, X. J.; Heinz, D. W.; Blaber, M.; Baldwin, E. P.; Matthews, B. W. *Science* **1992**, *255*, 178−183.
(30) Wong, K. K. W.; Whilton, N. T.; Coelfen, H.; Douglas, T.; Mann, S. *Chem. Commun.* **1998**, 1621−1622.
(31) Almiron, M.; Link, A. J.; Furlong, D.; Kolter, R. *Genes Dev.* **1992**, *6*, 2646−2654.
(32) Grant, R. A.; Filman, D. J.; Finkel, S. E.; Kolter, R.; Hogle, J. M. *Nat. Struct. Biol.* **1998**, *5*, 294−303.
(33) Zhao, G. H.; Ceci, P.; Ilari, A.; Giangiacomo, L.; Laue, T. M.; Chiancone, E.; Chasteen, N. D. *J. Biol. Chem.* **2002**, *277*, 27689−27696.
(34) Ilari, A.; Ceci, P.; Ferrari, D.; Rossi, G. L.; Chiancone, E. *J. Biol. Chem.* **2002**, *277*, 37619−37623.
(35) Martinez, A.; Kolter, R. *J. Bacteriol.* **1997**, *179*, 5188−5194.
(36) Azam, T. A.; Ishihama, A. *J. Biol. Chem.* **1999**, *274*, 33105−33113.
(37) Kim, J.; Yoshimura, S. H.; Hizume, K.; Ohniwa, R. L.; Ishihama, A.; Takeyasu, K. *Nucl. Acid Res.* **2004**, *32*, 1982−1992.
(38) Nair, S.; Finkel, S. E. *J. Bacteriol.* **2004**, *186*, 4192−4198.
(39) Santambrogio, P.; Pinto, P.; Levi, S.; Cozzi, A.; Rovida, E.; Albertini, A.; Artymiuk, P.; Harrison, P. M.; Arosio, P. *Biochem. J.* **1997**, *322*, 461−468.
(40) Wade, V. J.; Levi, S.; Arosio, P.; Treffry, A.; Harrison, P. M.; Mann, S. *J. Mol. Biol.* **1991**, *221*, 1443−1452.
(41) Kilic, M. A.; Spiro, S.; Moore, G. R. *Protein Sci.* **2003**, *12*, 1663−1674.
(42) Zeth, K.; Offermann, S.; Essen, L.-O.; Oesterhelt, D. *Proc. Natl. Acad. Sci. U.S.A.* **2004**, *101*, 13780−13785.
(43) Doerr, A. J.; Case, M. A.; Pelczer, I.; McLendon, G. L. *J. Am. Chem. Soc.* **2004**, *126*, 4192−4198.
(44) Bolon, D. N.; Mayo, S. L. *Proc. Natl. Acad. Sci. U.S.A.* **2001**, *98*, 14274−14279.
(45) Ghirlanda, G.; Osyczka, A.; Liu, W. X.; Antolovich, M.; Smith, K. M.; Dutton, P. L.; Wand, A. J.; DeGrado, W. F. *J. Am. Chem. Soc.* **2004**, *126*, 8141−8147.
(46) Dwyer, M. A.; Looger, L. L.; Hellinga, H. W. *Science* **2004**, *304*, 1967−1971.
(47) Calhoun, J. R.; Kono, H.; Lahr, S.; Wang, W.; DeGrado, W. F.; Saven, J. G. *J. Mol. Biol.* **2003**, *334*, 1101−1115.
(48) Kono, H.; Saven, J. G. *J. Mol. Biol.* **2001**, *306*, 607−628.
(49) Saven, J. G. *Curr. Opin. Struct. Biol.* **2002**, *12*, 453−458.
(50) Gillespie, B.; Vu, D. M.; Shah, P. S.; Marshall, S. A.; Dyer, R. B.; Mayo, S. L.; Plaxco, K. W. *J. Mol. Biol.* **2003**, *330*, 813−819.
(51) Kohn, J. E.; Plaxco, K. W. *Proc. Natl. Acad. Sci. U.S.A.* **2005**, *102*, 10841−10845.
(52) Kraemer-Pecore, C. M.; Lecomte, J. T. J.; Desjarlais, J. R. *Protein Sci.* **2003**, *12*, 2194−2205.
(53) Main, E. R. G.; Lowe, A. R.; Mochrie, S. G. J.; Jackson, S. E.; Regan, L. *Curr. Opin. Struct. Biol.* **2005**, *15*, 464−471.
(54) Southall, N. T.; Dill, K. A.; Haymet, A. D. J. *J. Phys. Chem. B* **2002**, *106*, 521−533.
(55) Dill, K. A. *Biochemistry* **1990**, *29*, 7133−7155.
(56) Korkegian, A.; Black, M. E.; Baker, D.; Stoddard, B. L. *Science* **2005**, *308*, 857−860.
(57) Kuhlman, B.; Dantas, G.; Ireton, G. C.; Varani, G.; Stoddard, B. L.; Baker, D. *Science* **2003**, *302*, 1364−1368.
(58) Kraemer-Pecore, C. M.; Wollacott, A. M.; Desjarlais, J. R. *Curr. Opin. Chem. Biol.* **2001**, *5*, 690−695.
(59) Discher, B. M.; Koder, R. L.; Moser, C. C.; Dutton, P. L. *Curr. Opin. Chem. Biol.* **2003**, *7*, 741−748.
(60) Cochran, F. V.; Wu, S. P.; Wang, W.; Nanda, V.; Saven, J. G.; Therien, M. J.; DeGrado, W. F. *J. Am. Chem. Soc.* **2005**, *127*, 1346−1347.
(61) Kaplan, J.; DeGrado, W. F. *Proc. Natl. Acad. Sci. U.S.A.* **2004**, *101*, 11566−11570.
(62) Looger, L. L.; Hellinga, H. W. *J. Mol. Biol.* **2001**, *307*, 429−445.
(63) Zou, J. M.; Saven, J. G. *J. Chem. Phys.* **2003**, *118*, 3843−3854.
(64) Park, S.; Xi, Y.; Saven, J. G. *Curr. Opin. Struct. Biol.* **2004**, *14*, 487−494.
(65) Zou, J. M.; Saven, J. G. *J. Mol. Biol.* **2000**, *296*, 281−294.
(66) Park, S.; Boder, E. T.; Saven, J. G. *J. Mol. Biol.* **2005**, *348*, 75−83.
(67) Park, S.; Kono, H.; Wang, W.; Boder, E. T.; Saven, J. G. *Comput. Chem. Eng.* **2005**, *29*, 407−421.
(68) Yang, X.; Saven, J. G. *Chem. Phys. Lett.* **2005**, *401*, 205−210.
(69) Fu, X. R.; Kono, H.; Saven, J. G. *Protein Eng.* **2003**, *16*, 971−977.
(70) Slovic, A. M.; Kono, H.; Lear, J. D.; Saven, J. G.; DeGrado, W. F. *Proc. Natl. Acad. Sci. U.S.A.* **2004**, *101*, 1828−1833.
(71) Nanda, V.; Rosenblatt, M. M.; Osyczka, A.; Kono, H.; Getahun, Z.; Dutton, P. L.; Saven, J. G.; DeGrado, W. F. *J. Am. Chem. Soc.* **2005**, *127*, 5804−5805.

Table 1. Mutations to Wild-Type *E. coli* Dps

protein	mutations
Dps3	E64V, D75V, R153V
Dps7	E64V, G68A, D75V, T79V, A150V, R153V, D154A
Dps10	E64V, G68A, T71V, D75V, T79V, D146Y, A150V, R153V, D154A, K157V

expressed and observed to form stable, hydrophobic cavity-containing Dps proteins of similar structure and function to the wild type.

Experimental Procedures

Computational Sequence Probabilities. The calculated site-specific amino acid probabilities at variable positions were determined as described previously.[47] A self-consistent statistical method[48] has been extended to address symmetrical structures,[69] facilitating calculations on systems the size of the Dps dodecamer. The calculations employ the Amber potential[72] with a modified hydrogen-bonding term.[73] Only hydrophobic amino acids (Ala, Gly, Ile, Leu, Phe, Trp, Tyr, and Val) were permitted at variable residues, and as a result, no solvation-related energy or scoring functions were used. All variable residues were permitted to mutate simultaneously. The remaining residues were fixed at wild-type identities, with the backbone and side-chain coordinates constrained to the side-chain conformations contained in the X-ray crystal structure of wild-type *E. coli* Dps (herein defined as DpsWT, PDB accession code 1DPS). Dps proteins having three, seven, and 10 hydrophobic mutations per four-helix bundle were defined as Dps3, Dps7, and Dps10, respectively. The mutation made at each of the highlighted residues is provided in Table 1.

Calculating Solvent-Accessible Apolar Surface Area. PDB files containing the designed mutations were generated for Dps3, Dps7, and Dps10 in PyMol.[74] Apolar and polar surface area calculations were performed for each Dps protein using GETAREA[75] with a 1.4 Å water probe and standard atomic solvation parameters. Apolar and polar surface areas were calculated on a per amino acid basis and summed for the solvent-accessible residues that lined the cavity (60, 61, 63−65, 67−72, 74−79, 82, 83, 85, 86, 146, 147, 149, 150, 153, 154, and 156−161).

Starting Materials. All chemicals were of analytical reagent grade and used as purchased without further purification. Tryptone peptone and yeast extract were purchased from Difco. L-arabinose, protamine sulfate, and ampicillin were purchased from Sigma. TEMED, 30% acrylamide, ammonium persulfate, and BioSafe Coomassie Stain for gel electrophoresis were purchased from Bio-Rad. UltraPure guanidine hydrochloride (GuHCl) was purchased from Invitrogen. Unless otherwise noted, all other chemicals were purchased from Fisher Scientific and were of certified ACS grade or better. All solutions were prepared using deionized water purified by Ultrapure Water Systems. The standard buffer is defined herein as 50 mM sodium phosphate, 500 mM NaCl, pH 8.

Protein Expression and Purification. Dps mutants were constructed using the Stratagene QuikChange MultiSite kit to generate a family of hydrophobic cavity proteins. The pBAD18 vector containing each Dps gene was transformed into a BL21(DE3) cell strain of *E. coli* (Novagen). Cell cultures were grown in LB medium (1.5 L volume, 10 g/L NaCl, 10 g/L tryptone, 5 g/L yeast, pH 7) supplemented with 200 μg/mL ampicillin at 37 °C to mid-log phase ($OD_{560} \sim 1.0$). Protein expression was then induced for 4 h at 37 °C using 5 mM L-arabinose. All subsequent manipulations were performed at 4 °C. Cells were harvested by centrifugation and resuspended in 50 mL of standard buffer containing a protease inhibitor cocktail tablet (Roche Diagnostics GmbH). The cells were then sonicated in three 2 min cycles. Cell debris and denatured protein were removed by centrifugation. Protamine sulfate (100 mg) was added, and the resulting coprecipitate of protamine and nucleic acids was removed by centrifugation and discarded. Further impurities were precipitated with a 50% ammonium sulfate cut, pelleted by centrifugation, and discarded. The Dps proteins were precipitated with a 90% ammonium sulfate cut, which was pelleted by centrifugation and then resuspended in minimum buffer. Dps was purified on a HiPrep 26/60 Sephacryl S-300 HR size-exclusion column operated by an Amersham Biosciences Äkta UPC900/P-920 FPLC running with a high ionic strength buffer (2 M NaCl, 50 mM Tris, pH 8) to allow separation of the protein from DNA. The Dps fractions were combined, concentrated, and run a second time through the same column to yield protein of greater than 95% purity. For Dps7 and Dps10, all steps were carried out as described for DpsWT and Dps3, with the difference that Dps7 and Dps10 were induced at 20 °C for 8 h.

Gel Electrophoresis, UV−vis, MALDI-TOF, Circular Dichroism (CD). Protein purity was assayed by SDS−PAGE (15% resolving, 5% stacking) gels. Samples were prepared by taking 10 μL of 1 mg/mL protein solution, mixing with 20 μL of running buffer, and boiling for 5 min. Samples (15 μL) were then loaded alongside a lane of Bio-Rad SDS−PAGE Broad Range standards. The gel was run at 200 V before staining. The developed gel was imaged on a Bio-Rad Gel Doc 2000 system, and the bands were integrated using Quantity One v4.5 software (Bio-Rad).

Dps samples were analyzed by UV−vis spectroscopy with an Agilent 8453 spectrophotometer with a temperature controller and magnetic stirrer (Agilent 89090A), using a quartz cuvette with a 1 cm path length. The molecular weights of the Dps four-helix bundle subunits were determined at the Wistar Institute Proteomics Facility using an Applied Biosystems Voyager System 6030 MALDI-TOF mass spectrometer. CD spectra were collected on an Aviv 62DS spectropolarimeter in the wavelength range of 190−260 nm (far UV) and from 260 to 350 nm (near UV) using a 1 mm quartz cell. Protein samples were prepared at 0.1 mg/mL in standard buffer.

Dynamic Light Scattering (DLS). Hydrodynamic radii for Dps samples (0.1 mg/mL in standard buffer) were determined using a DynaPro 99 (ProteinSolutions, Inc., Charlottesville, VA). The data were analyzed, and histograms were generated using Dynamics 5.26.37 software (ProteinSolutions).

Thermal and GuHCl Denaturation. Samples for thermal denaturation were prepared with 0.1 mg/mL protein in standard buffer. Ellipticity was measured at 222 nm by CD, and the temperature was increased from 4 to 96 °C in 4° steps. The melting process resulted in a loss of signal as the secondary structure was lost and the protein precipitated from solution. The samples were allowed to equilibrate for 5 min at each temperature. Melting temperatures were determined from the maximum of the first derivative plot of % unfolded versus inverse temperature.

Samples for GuHCl denaturation were prepared with 0.1 mg/mL protein and concentrations of GuHCl varying between 0 and 7 M in standard buffer. The samples were mixed by vortex and allowed to stand at 4 °C overnight, to achieve the maximum denaturation at each guanidine concentration. Previous unpublished work by this group using a stopped-flow apparatus found that Dps folding and unfolding events occurred on a time scale significantly shorter than 12 h. Ellipticity was measured at 222 nm by CD. The ratio of Trp fluorescence at 316 nm/348 nm was determined with a Fluorolog 3.10 spectrophotometer (Jobin Yvon Horiba, NJ) with a 2 nm resolution and a 1 cm quartz sample holder, upon excitation at 295 nm.

Kinetics of Iron Mineralization. Aerobic iron mineralization experiments were performed by adding 150 equiv of Fe^{2+} from a freshly prepared anaerobic ferrous ammonium sulfate solution (68 mM) to air-equilibrated solutions of newly purified protein (0.1 mg/mL, 0.45 mM,

(72) Weiner, S. J.; Kollman, P. A.; Case, D. A.; Singh, U. C.; Ghio, C.; Alagona, G.; Profeta, S.; Weiner, P. *J. Am. Chem. Soc.* **1984**, *106*, 765−784.
(73) Kono, H.; Doi, J. *J. Comput. Chem.* **1996**, *17*, 1667−1683.
(74) DeLano, W. L. *The PyMOL User's Manual*; DeLano Scientific: San Carlos, CA, 2002.
(75) Fraczkiewicz, R.; Braun, W. *J. Comput. Chem.* **1998**, *19*, 319−333.

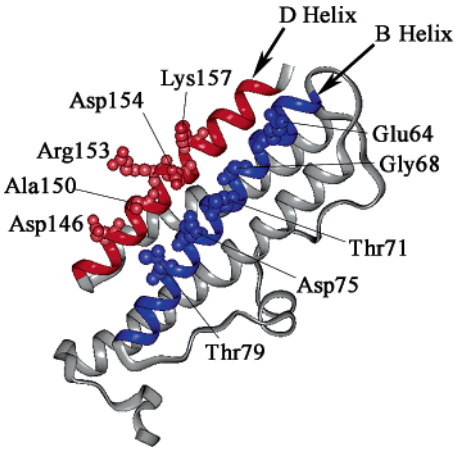

Figure 1. Four-helix bundle structure of the DpsWT monomer highlighting the B (blue) and D (red) helices. Labels identify 10 solvent-accessible hydrophilic residues that were mutated.

as determined by Bradford assay), in 50 mM MOPS, 500 mM NaCl, pH 7.3. The kinetics of iron oxidation and uptake were followed at 25 °C by measuring at 1 s intervals the absorbance of the iron mineral at 310 nm. Data were collected with UV−vis ChemStation software (Rev. A.09.01, Agilent). The data points were averaged over 8 s intervals to reduce noise and spikes and then averaged over three runs. The resulting curves were fitted to single exponential functions using IgorPro (Version 4.0, Wavemetrics). The solutions were continuously stirred during the course of the experiments. As a control, the rate of Fe^{2+} autoxidation was measured in the absence of protein.

Anaerobic iron mineralization experiments were performed by adding 50 equiv of Fe^{2+} (15 mM, prepared anaerobically as described previously) followed by 100 equiv of H_2O_2 (30 mM) to degassed solutions of newly purified protein (0.075 mg/mL, 0.30 mM), in 50 mM MOPS, 500 mM NaCl, pH 7.3. The kinetics were followed and analyzed as described for aerobic conditions, with the exception that a double exponential function was fitted to the data. Solutions were continuously stirred under anaerobic conditions. The rate of oxidation was measured in the presence of peroxide but the absence of protein.

Maximal Iron Loading. Anaerobic iron mineralization experiments were performed by adding aliquots of 100 equiv of Fe^{2+} from a freshly prepared anaerobic ferrous ammonium sulfate solution (15 mM), followed by 100 equiv of H_2O_2 (15 mM), to degassed solutions of newly purified protein (0.075 mg/mL, 0.45 mM, as determined by Bradford assay), in 50 mM MOPS, 500 mM NaCl, pH 7.3. Samples were equilibrated under a constant pressure of argon gas for 20 min, and a UV−vis spectrum was taken before adding more iron.

Results

Protein Design. Previous mutagenesis studies in recombinant human ferritin[41] and bacterioferritin[39] examined the effect of changing residues at the two-, three-, and four-fold symmetry axes on subunit assembly. To maintain the stability of the assembled Dps holoprotein, while maximizing the hydrophobicity of the cavity, we avoided any changes at these important subunit interfaces. In re-engineering Dps, 14 hydrophilic residues were identified in each subunit with greater than 15% solvent exposure on the interior surface of the protein. Of these, it was determined that 10 residues could be substituted directly without destabilizing contacts within or between the four-helix bundles (Figure 1). Cut-away projections of the interior cavities of DpsWT and Dps10, based on a previously published crystal structure (PDB code 1DPS), are shown for comparison (Figure 2). The site-specific probabilities of eight hydrophobic amino acids (Ala, Gly, Ile, Leu, Phe, Trp, Tyr, and Val) were determined at each site (B-Helix, Glu64, Gly68, Thr71, Asp75, and Thr79 and D-Helix, Asp146, Ala150, Arg153, Asp154, and Lys157). It was determined through inspection of the Dps crystal structure that mutating other polar amino acids, Asp67, Arg70, and Asp78, may adversely impact several salt bridges in the hydrophobic core; therefore, these mutations were not attempted.

The site-specific probability of each hydrophobic amino acid was calculated at each position using a statistically based computational design strategy,[47,48,69] yielding mutations consistent with the structure of the wild-type protein. The probabilities of hydrophobic residues indicated that some sites on the B- and D-helices (75, 150, 153, 154, and 157) were well-determined, while others (64, 68, 71, 79, and 146) tolerated multiple substitutions (Figure 3). Using these amino acid probabilities, sequences comprising increasing numbers of mutations were identified for experimental characterization: Dps3, Dps7, and Dps10 (see Table 1). The percentage of the solvent-accessible surface area inside the cavity that was occupied by apolar amino acids increased considerably with each round of mutations, as calculated by GETAREA:[75] 52% for DpsWT, 69% for Dps3, 77% for Dps7, and 86% for Dps10.

Protein Characterization. All four Dps proteins eluted at 152 ± 2 mL on a Sephacryl S-300 size-exclusion column (Figure 4). This retention volume was consistent with the elution of a dodecameric, fully assembled, 220 kD protein, based upon calibration of the column with proteins of known molecular weight (Figure 5). As indicated by the small absorbance peak for Dps10, this mutant could not be isolated in the pure form in sufficient quantities for complete biophysical characterization. Gel electrophoresis (SDS−PAGE) and UV−vis spectroscopy showed all four proteins to be at least 95% pure. An extinction coefficient of $(2.1 \pm 0.2) \times 10^5$ M^{-1} cm^{-1} at 280 nm was determined for Dps using a Bradford assay. All Dps holoproteins initially associated with DNA, which was removed during the purification process. MALDI-TOF mass spectrometry confirmed the identity of the individual Dps subunits (Table 2). Far UV circular dichroism (Figure 6) showed that the secondary structure was highly conserved for DpsWT, Dps3, and Dps7 (89% α-helical), while Dps10 was only slightly less α-helical (85%). The values for percent α-helical character shown in Table 2 were estimated using eq 1[76−78]

$$f_H = \frac{[\theta]_{222}}{[\theta_\infty]_{222}} \quad (1)$$

where $[\theta]_{222}$ is the ellipticity at 222 nm, $[\theta_\infty]_{222}$ is the mean residue ellipticity of an ideal peptide with 100% helicity (set to −44 000 deg cm^2 $dmol^{-1}$). An analysis of the Dps crystal structure suggests that eq 1 over-estimates the % helicity.

Trp fluorescence, near UV CD, and DLS measurements probed the assembled state of each protein. The Dps subunits contained two tryptophans, W52 and W160. Dps assembly placed these tryptophans at the subunit interfaces, thereby burying them from solvent. Thus, fluorescence from W52 and W160 reported sensitively on the state of subunit assembly.

(76) Chen, Y. H.; Yang, J. T.; Chau, K. H. *Biochemistry* **1974**, *13*, 3350−3359.
(77) Gans, P. J.; Lyu, P. C.; Manning, M. C.; Woody, R. W.; Kallenbach, N. R. *Biopolymers* **1991**, *31*, 1605−1614.
(78) Luo, P.; Baldwin, R. L. *Biochemistry* **1997**, *36*, 8413−8421.

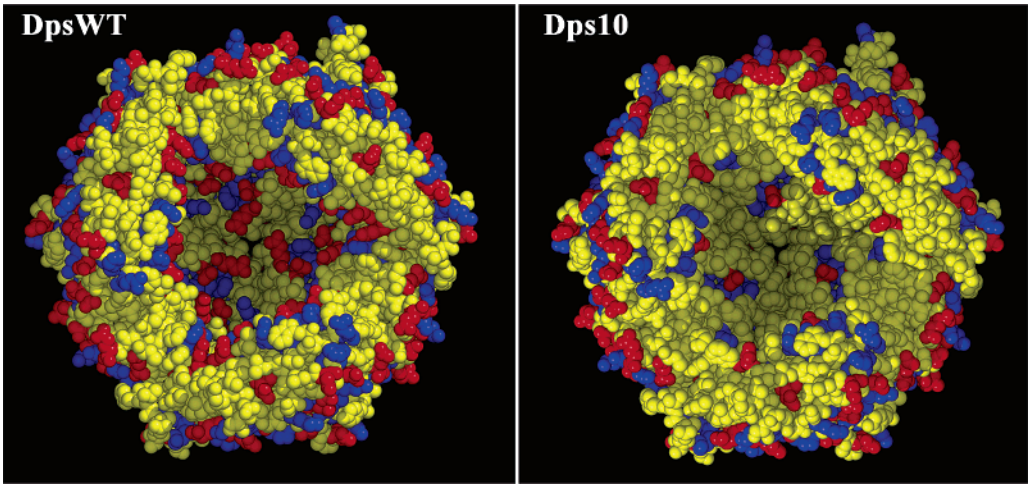

Figure 2. Cut-away views showing the interior of DpsWT (from the crystal structure)[32] and Dps10 (model based on the crystal structure). Hydrophobic residues are indicated in yellow, acidic residues in red, and basic residues in blue.

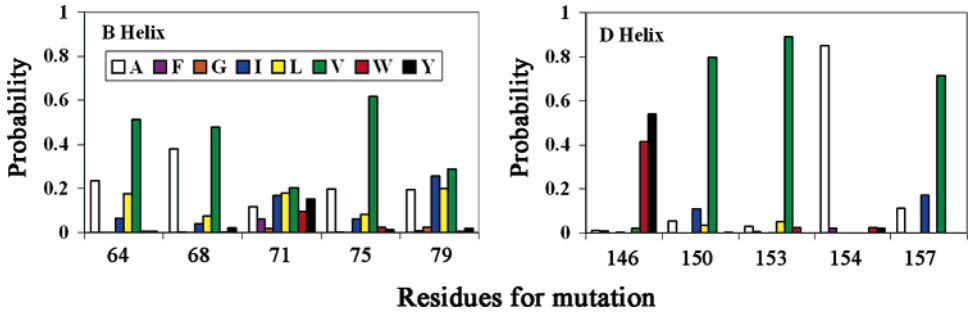

Figure 3. Probabilities for incorporating each of eight different hydrophobic residues at 10 solvent-accessible sites on the B and D helices.

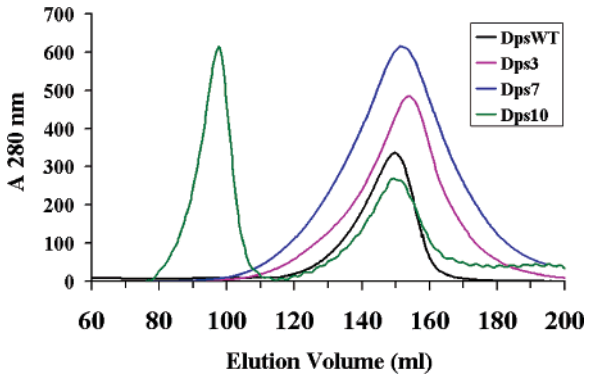

Figure 4. Fast protein liquid chromatography (FPLC) traces showing elution of the Dps proteins at approximately 152 mL. Samples before purification contained both Dps and DNA, which eluted in the first peak at ~95 mL. FPLC data were recorded with the UV-vis detector set to 280 nm while the running buffer (2 M NaCl, 50 mM Tris, 1 mM EDTA, pH 8) was at 0.2 mL/min. The absorbance of the Dps10 trace is multiplied by 100 so it appears on the same scale as the other proteins.

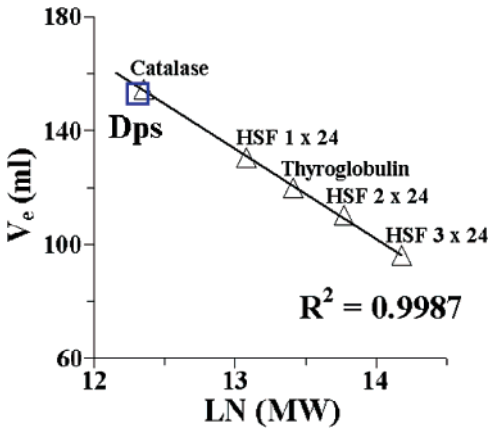

Figure 5. Calibration plot for the Sephacryl S-300 FPLC column, showing that the elution of the Dps proteins at 152 mL was consistent with a molecular weight of 220 kD, which corresponds to the intact dodecamer.

Photoexcitation at 295 nm gave virtually identical fluorescence spectra for all Dps proteins (Figure 7A), with $\lambda_{max} = 336$ nm in phosphate buffer, indicating similar modes of subunit assembly. A similar tryptophan environment in the three proteins was also demonstrated by near UV CD spectroscopy (Figure 7B). Further evidence for the formation of the holoprotein was provided by dynamic light scattering experiments: proteins were identified with radii of 5.1 ± 0.9 nm for DpsWT; 4.6 ± 0.8 nm for Dps3; and 4.9 ± 1.1 nm for Dps7. The formation of these homogeneous, 9−10 nm diameter particles in solution was in excellent agreement with published X-ray crystallographic data for wild-type Dps.[32,79]

DpsWT, Dps3, and Dps7 exhibited very similar melting temperatures, $T_m \sim 90$ °C (Table 2), where the loss in ellipticity at 222 nm with increasing temperature was measured by CD (Figure 8). Even in the more hydrophobic Dps10 mutant, the thermal stability was quite high, $T_m = 74$ °C. Thermal melting in the Dps proteins was not completely reversible due to precipitation at high temperatures, as evidenced by the loss in secondary structure and the solutions becoming slightly turbid. This likely resulted from irreversible aggregation of unfolded polypeptides, which is a common phenomenon with heat

(79) Ren, B.; Tibbelin, G.; Kajino, T.; Asami, O.; Ladenstein, R. *J. Mol. Biol.* **2003**, *329*, 467−477.

Table 2. Physical Characterization of Dps Proteins

protein	MW (calc)	MW (exptl)	helicity (%)	T_m (°C)	radius (nm)	$[GuHCl]_{1/2}$ (M)	$\Delta G_f^{H_2O}/n$ (kJ per mol subunit)	apolar surface (Å^2) (%) [a]
DpsWT	18578.9	18579	89	90	5.1 ± 0.9	3.76	101 ± 3	5760 (52)
Dps3	18475.9	18470	89	87	4.6 ± 0.8	2.23	45 ± 2	7630 (69)
Dps7	18472.0	18467	89	89	4.9 ± 1.1	1.47	38 ± 1	8610 (77)
Dps10	18489.1	18491	85	74	N/D	N/D	N/D	9550 (86)

[a] Percent of the total interior solvent-accessible surface area that was classified as apolar using GETAREA.[75]

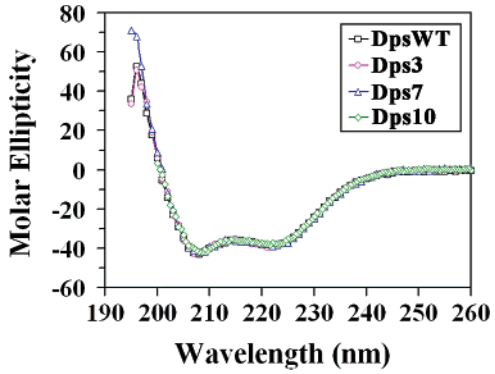

Figure 6. Molar ellipticity ($[\theta] \times 10^{-3}$ deg cm^2 dmol^{-1}) of Dps proteins measured by far UV CD. Recorded at a protein concentration of 0.1 mg/mL in standard buffer.

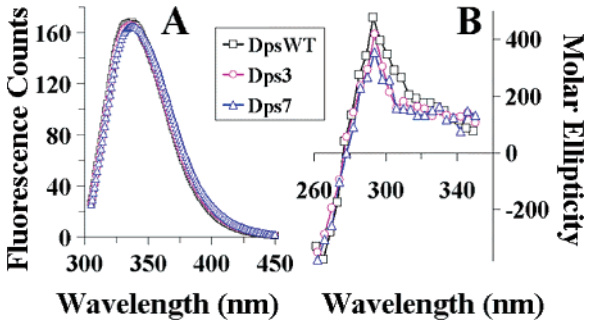

Figure 7. (A) Fluorescence spectra of Dps proteins excited at 295 nm. Recorded at a protein concentration of 0.1 mg/mL in standard buffer. (B) Molar ellipticity ($[\theta] \times 10^{-6}$ deg cm^2 dmol^{-1}) of Dps proteins measured by near UV CD. Recorded at a protein concentration of 0.2 mg/mL in standard buffer.

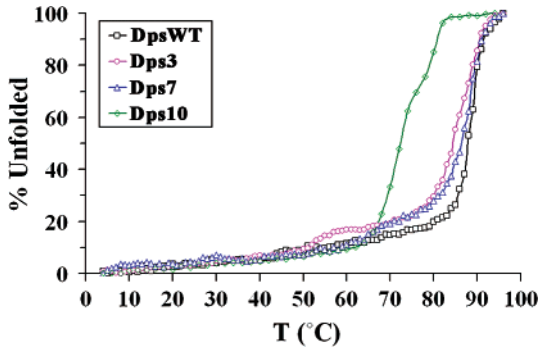

Figure 8. Thermal denaturation of Dps proteins, with % unfolded calculated from the change in CD signal at 222 nm; 0.1 mg/mL protein in standard buffer.

denaturation of multimeric proteins.[80] Indeed, this behavior was observed previously for horse spleen and human ferritins,[81] as well as bacterioferritin.[41] However, DpsWT, Dps3, and Dps7 could be heated to 75 °C without any loss of protein. This agreed with previous experiments showing reversible partial denaturation when the ferritins were heated to 5−10 °C below their T_m values.[81] Even at room temperature, protein aggregation was evident at acidic pH, but this was avoided by working at pH values between 7.5 and 8.0 and at low protein concentrations (<1 mg/mL). Problems with solubility at acidic pH have been linked to the N-terminal lysine residues (K5, K8, K10), which play an important role in Dps self-aggregation, as well as DNA binding.[82]

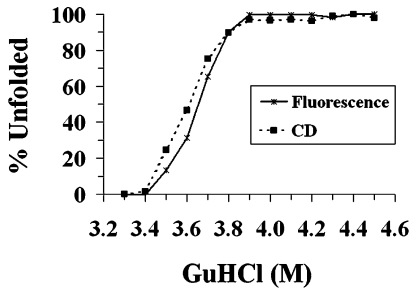

Figure 9. GuHCl unfolding of DpsWT at room temperature monitored by changes in Trp fluorescence at two wavelengths (I_{316nm} and I_{348nm}) and CD (changes in ellipticity at 222 nm). Unfolding was completely reversible by diluting the concentration of GuHCl (not shown).

To further explore increased hydrophobicity, Dps11 was generated by replacing Glu82 with tryptophan, as suggested by computational design. This protein was expressed in low yield, was poorly soluble, and could not be isolated in a pure form. Recent evidence from a crystal structure of a related Dps protein showed that the residue corresponding to E82 binds metal ions at an intersubunit ferroxidase site.[83] Thus, removing this ligand may have destabilized the holoprotein.

The unfolding of DpsWT due to GuHCl (Figure 9) was monitored by changes in Trp fluorescence (at 316 and 348 nm) and ellipticity (CD signal at 222 nm). Protein unfolding and refolding were completely reversible over a broad range of GuHCl concentrations (0−7 M). The percentage of unfolded protein was calculated by measuring the ratio of Trp fluorescence intensities at two wavelengths, $R = I_{316nm}/I_{348nm}$, in both the completely folded (R_f) and unfolded (R_u) regimes: % unfolded $= [(R_f - R)/(R_f - R_u)] \times 100$. The unfolding and refolding transitions for DpsWT occurred over a narrow range of denaturant concentrations (3.4−3.8 M GuHCl at pH 8). The transition appears particularly sharp when compared with data for Dps 3 and Dps7 (Figure 10). GuHCl denaturation of Dps7 was consistent with the population of at least one intermediate species, based on the shoulder in Figure 10 at GuHCl concentrations between 1.7 and 3.1 M.

(80) Jaenicke, R. *Prog. Biophys. Mol. Biol.* **1987**, *49*, 117−237.
(81) Stefanini, S.; Cavallo, S.; Wang, C.-Q.; Tataseo, P.; Vecchini, P.; Giartosio, A.; Chiancone, E. *Arch. Biochem. Biophys.* **1996**, *325*, 58−64.
(82) Ceci, P.; Cellai, S.; Falvo, E.; Rivetti, C.; Rossi, G. L.; Chiancone, E. *Nucleic Acids Res.* **2004**, *32*, 5935−5944.
(83) Ilari, A.; Stefanini, S.; Chiancone, E.; Tsernoglou, D. *Nat. Struct. Biol.* **2000**, *7*, 38−43.

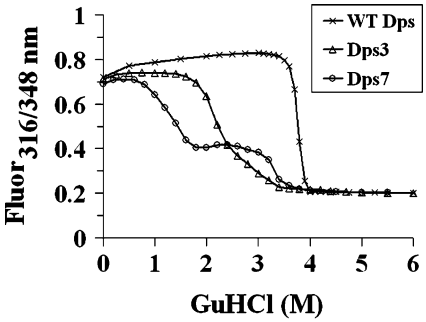

Figure 10. GuHCl unfolding of DpsWT, Dps3, and Dps7 at room temperature monitored by changes in the ratio of Trp fluorescence at two wavelengths (I_{316nm}/I_{348nm}); 0.1 mg/mL protein in standard buffer.

Dps subunits fold and oligomerize to form an *n*-mer, where $n = 12$. DpsWT and Dps3 exhibited a highly cooperative subunit assembly, as evidenced by the fact that unfolding with GuHCl gave no intermediates detectable by the equilibrium methods used in this work (Figure 10). Thus, oligomerization was treated using a simple model with the following assumptions: (1) intermediate oligomerization states with *m* subunits ($m < n$) were essentially unpopulated and (2) only folded Dps formed the 12-mer. On the basis of this model, equilibrium constants were established for Dps folding and assembly. In the all-or-none folding and assembly scenario, all of the Trp fluorescence associated with the Dps folded state was assigned to the 12-mer. From these conditions, eq 2 was derived

$$\Delta G_f = -RT \ln(f_{Ft}/(nf_U)) + (n-1)RT \ln(f_U P_t) \qquad (2)$$

where ΔG_f is the free energy of folding the 12-mer, f_{Ft} is the fraction of total folded protein present as both the monomer and oligomer, $f_U = 1 - f_{Ft}$ is the fraction of unfolded protein, and P_t is the total concentration of protein in mol/L. The free energy of folding in water, $\Delta G_f^{H_2O}$, was estimated by assuming that the linear dependence of ΔG_f observed at high GuHCl concentrations in the transition region continued to zero denaturant concentration.[41,84,85]

To calculate ΔG_f, straight lines were first fitted to the fully folded and fully unfolded regions of the denaturation curves. The extent of unfolding at all intermediate GuHCl concentrations was then evaluated, and ΔG_f at each guanidine concentration was calculated using eq 2. Values were also calculated for $\Delta G_f/n$, to determine the stability of the holoprotein on a per subunit basis. Graphs of $\Delta G_f/n$ against GuHCl concentration for DpsWT and Dps3 showed linear relationships (Figure 11): straight-line fits for DpsWT and Dps3 data gave R^2 values of 0.99 and 0.83. Extrapolating to [GuHCl] = 0 M allowed $\Delta G_f^{H_2O}/n$ to be obtained (Table 2). Dps7 was also included in this analysis, although it showed at least one intermediate state comprised of some number of subunits, which is reflected in a lower R^2 value of 0.69. The $\Delta G_f^{H_2O}/n$ values estimated for DpsWT (101 ± 3 kJ per mol of subunit), Dps3 (45 ± 2 kJ per mol of subunit), and Dps7 (38 ± 1 kJ per mol of subunit) decreased with increasing hydrophobicity; nonetheless, Dps3 and Dps7 remained quite stable to denaturant, considering the large number of mutations.

Iron Mineralization Studies. The addition of 150 equiv of Fe^{2+} to the Dps proteins under aerobic conditions led to an absorbance increase at 310 nm. Straight lines were fit to the initial data points to find a rate for iron oxidation and mineralization. Figure 12A shows that for DpsWT and Dps7 under the described experimental conditions, the rates of iron mineralization were virtually identical within experimental error, and the absorbance recorded at the end of the reaction was approximately 0.16 at 310 nm, which indicated the formation of iron mineral cores of similar size. On the basis of this value, the molar absorptivity for the oxidation product was determined to be $\epsilon_{310nm} = 2300 \pm 100\ M^{-1}\ cm^{-1}$ per iron, which is typical for mineralized ferric iron inside ferritin proteins.[33,86,87] All

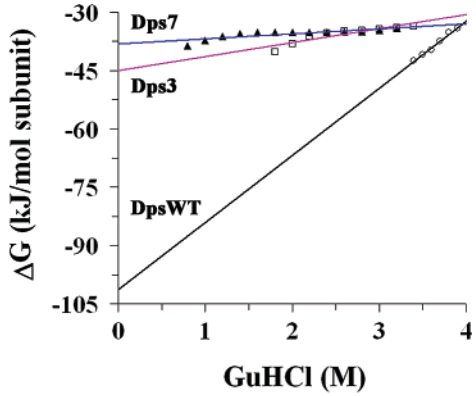

Figure 11. Dependence of the free energy of folding of the DpsWT, Dps3, and Dps7 holoproteins as a function of the concentration of GuHCl, calculated on a per subunit basis, $n = 12$. Linear extrapolation to 0 M GuHCl gave the free energy change per mol of subunit in the absence of denaturant, $\Delta G_f^{H_2O}/n$. Solid lines were obtained from least-squares fitting.

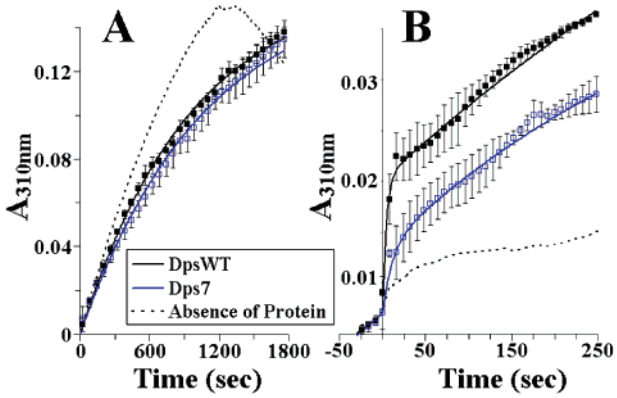

Figure 12. (A) Iron mineralization by Dps proteins under aerobic conditions after addition of 150 equiv of Fe^{2+}; 0.1 mg/mL protein, in 50 mM MOPS, 500 mM NaCl at pH 7.3. Data were averaged from three runs and fit to a single-exponential function, weighted to the standard deviation, using Wavemetrics' IgorPro 4. The initial rates of mineralization in DpsWT (0.38 Fe^{3+} holoprotein^{-1} s^{-1}) and Dps7 (0.35 Fe^{3+} holoprotein^{-1} s^{-1}) were found to be similar. The apparent high initial rate of autoxidation reflects light scattering by Fe(III) hydroxide particles; these particles eventually precipitated. No precipitation was observed in the protein assays. (B) Iron mineralization by Dps proteins under anaerobic conditions after addition of 50 equiv of Fe^{2+} followed by the addition of 100 equiv of H_2O_2 (injected at time = 0 s), 0.075 mg/mL protein, in 50 mM MOPS, 500 mM NaCl at pH 7.3. Data were averaged from three runs and fitted to a double exponential, weighted to the standard deviation, using IgorPro 4. A control was run with peroxide added to the iron solution without the presence of protein. Mineralization by Dps7 (3.2 Fe^{3+} holoprotein^{-1} s^{-1}) was found to be slower than by DpsWT (7.1 Fe^{3+} holoprotein^{-1} s^{-1}), but both were considerably faster than oxidation in the absence of protein.

(84) Jackson, S. E.; Fersht, A. R. *Biochemistry* **1991**, *30*, 10428−10435.
(85) Pace, C. N. *Methods Enzymol.* **1986**, *131*, 266−280.
(86) Meihong, S.; Cavallo, S.; Stefanini, S.; Chiancone, E.; Chasteen, N. D. *Biochemistry* **2005**, *44*, 5572−5578.
(87) Yang, X.; Chen-Barrett, Y.; Arosio, P.; Chasteen, N. D. *Biochemistry* **1998**, *37*, 9743−9750.

proteins complexed with iron were soluble during the course of the mineralization experiments, whereas in the absence of protein, autoxidized iron precipitated out of solution. The rate of autoxidation was found to be comparable to that of Dps-mediated iron mineralization.

Iron mineralization by DpsWT and Dps7 was also monitored under anaerobic conditions upon addition of 50 equiv of Fe^{2+}, followed by the addition of 100 equiv of H_2O_2. Mineralization by Dps7 (3.2 Fe^{3+} holoprotein^{-1} s^{-1}) was found to be slower than by DpsWT (7.1 Fe^{3+} holoprotein^{-1} s^{-1}), but both were considerably faster than iron oxidation in the absence of protein (Figure 12B).

Steady-state maximal iron loading experiments were performed under anaerobic conditions using hydrogen peroxide as the oxidant, in both DpsWT and Dps7. These studies showed the formation of a mineral core with approximately 500 Fe^{3+} atoms per DpsWT holoprotein and approximately 300 Fe^{3+} atoms per Dps7 holoprotein. The UV−vis spectrum for iron-loaded Dps7 was almost identical to that of DpsWT under both aerobic and anaerobic conditions, the only difference being a slight suppression of the maxima at 230 nm in the case of Dps7. Toward the end of the anaerobic kinetic runs, a shoulder was observed at 267 nm in both the DpsWT and Dps7 experiments; we tentatively assign this to the slow formation of an iron-peroxide species. UV−vis spectra of iron-loaded Dps are included in the Supporting Information.

Discussion

DpsWT exhibited exceptionally cooperative protein folding and unfolding as compared to other wild-type ferritin-like proteins. Thermal denaturation occurred over a narrow temperature range (85−95 °C), which is remarkable considering the size and complexity of this protein assembly. Unfolding experiments with DpsWT were expected to show subunit disassembly (monitored by Trp fluorescence) and subsequently loss of helical protein structure (monitored by CD) with increasing GuHCl concentration. In fact, both processes in DpsWT occurred over the same narrow range of guanidine concentrations (Figure 9), in both the folding and the unfolding directions. This confirmed the high cooperativity of subunit assembly and justified analyzing the stability of DpsWT to GuHCl using a modified two-state model (eq 2).[88] In the 24-mer homopolymer bacterioferritin, a similar observation was made that disruption of quaternary structure occurred with the loss of α-helical character.[41] Interestingly, with only 12 subunits, wild-type Dps exhibited a much sharper unfolding transition than bacterioferritin[41] or recombinant H and L human ferritins.[39] This improved the accuracy of determining $\Delta G_f^{H_2O}/n$ by the graphical linear extrapolation method (Figure 11).

Dps3 unfolded over a broader range of denaturant concentrations (1.5−4 M GuHCl), which is typical of ferritin proteins, and gave no evidence of partially assembled intermediates. Dps7, however, showed very different unfolding behavior with a partially folded intermediate in the range of 1.7−3.1 M GuHCl. The thermal melting experiment for Dps10 also deviated from linearity (Figure 8), which indicated the population of an unfolded state ensemble. Partially assembled ferritin species have been observed previously, including in the D131I + E134F mutant of recombinant human ferritin[39] and in Dps from *Mycobacterium smegmatis*,[89,90] which has stable dimeric, trimeric, and dodecameric forms. Future computational design can play a role in dissecting the interactions involved in stabilizing these four-helix bundle assemblies.

The Gibbs free energy changes of folding calculated for DpsWT, Dps3, and Dps7 do not address the large number of intermediate associated states (dimers, dimers of dimers, and nonspecific multimers) that can be formed by the 12 subunits under partially denaturing conditions. Additional means of characterizing stability are useful. Another general indicator of stability was provided by measuring the concentration of GuHCl at which half of each protein was unfolded, $[GuHCl]_{1/2}$ (Table 2). $[GuHCl]_{1/2}$ decreased as the proteins became increasingly hydrophobic: 3.76 M for DpsWT, 2.23 M for Dps3, and 1.47 M for Dps7. This trend, combined with the observed difficulty of isolating pure Dps10, suggests that there may be a finite limit to the solvent-accessible hydrophobicity of the protein cavity. We are not aware of any similarly large, enclosed hydrophobic protein cavities occurring in nature, although the hydrophobic surface area is reminiscent of some membrane-bound pore-forming proteins, such as the anthrax toxin[91] as well as protein-folding chaperone proteins.[92]

Future efforts to substitute residues inside the Dps cavity could consider other possible sets of mutations, to maximize the stability of the individual four-helix bundles. Mutation of some valine residues to other amino acids having higher helical propensities may increase the overall protein stability. Mutations at solvent-accessible residues on the outer protein surface are likely to have an even greater effect in stabilizing the dodecamer.[47,70] By stabilizing the holoprotein in this way, it may be possible to generate ferritin-like proteins with interior surface areas that are greater than 90% apolar.

Functional studies of iron mineralization indicated that the removal of key iron-binding residues within the Dps7 cavity diminished both the rate of peroxide-mediated iron loading as well as the total number of iron atoms stored within the protein. One possible explanation for this difference is that multiple points of attachment within the Dps cavity are required for rapid mineral growth. Interestingly, the mutations seemed to have very little effect on iron binding in aerobic conditions, where the increase in absorption at 310 nm proceeded at a rate comparable to autoxidation. A similar result was observed by Ilari et al.,[93] where a series of mutations to the ferroxidase center of *Listeria innocua* Dps was found to have a limited effect on the kinetics of loading, which were again similar to autoxidation. We hypothesize that the presence of iron-binding residues is relatively unimportant to the aerobic mineralization process, where readily oxidized iron may be sequestered by the protein before aggregation and precipitation occurs. The close agreement of the absorption spectra of the iron minerals formed from

(88) Pace, C. N.; Scholtz, J. M. In *Protein structure: A practical approach*, 2nd ed.; Creighton, T. E., Ed.; IRL Press: Oxford, UK, 1997; pp 299−321.
(89) Gupta, S.; Chatterji, D. *J. Biol. Chem.* **2003**, *278*, 5235−5241.
(90) Ceci, P.; Ilari, A.; Falvo, E.; Giangiacomo, L.; Chiancone, E. *J. Biol. Chem.* **2005**, *280*, 34776−34785.
(91) Krantz, B. A.; Melnyk, R. A.; Zhang, S.; Juris, S. J.; Lacy, D. B.; Wu, Z.; Finkelstein, A.; Collier, R. J. *Science* **2005**, *309*, 777−781.
(92) Maier, T.; Ferbitz, L.; Deuerling, E.; Ban, N. *Curr. Opin. Struct. Biol.* **2005**, *15*, 204−212.
(93) Ilari, A.; Latella, M. C.; Ceci, P.; Ribacchi, F.; Su, M.; Giangiacomo, L.; Stefanini, S.; Chasteen, N. D.; Chiancone, E. *Biochemistry* **2005**, *44*, 5579−5587.

DpsWT and Dps7 under either aerobic or anaerobic conditions suggests that the mutations do not perturb the structure and composition of the mineral deposit.

Conclusion

The present study illustrates the tremendous synthetic flexibility of the ferritin self-assembling, four-helix bundle motif. Computational design generated Dps proteins that deviated greatly from the native sequence. These mutations reduced the polarity of the large interior cavity, while maintaining the propensity of the Dps monomers to self-assemble and form a stable holoprotein. The melting temperatures of Dps3 and Dps7 were almost unchanged from the wild-type protein, indicating that these mutants maintained a high thermal stability. Dps10 was shown to still fold and assemble properly. The stability of related ferritin-like proteins may be optimized through additional rounds of computational design and protein characterization. Dps7 maintained near-native function, with a comparable rate of iron mineralization to DpsWT under aerobic conditions and approximately half the rate of iron deposition in the presence of H_2O_2.

Ferritins are ideally suited for the design of nanoreactors since the proteins vary considerably between species, modifications of the individual four-helix bundles are amplified 12- or 24-fold through the process of self-assembly, and these proteins can be characterized at atomic resolution by X-ray crystallography. The malleability of ferritin-like proteins seems to arise from the large number of ionic and hydrophobic interactions between the individual four-helix bundles that stabilize the holoprotein.[39,41] Extending this work to ferritin heteropolymers will allow subunits with different properties to be mixed in different stoichiometries,[94] to tailor the properties of the cavity. These studies with hydrophobic mutants, which should be prone to aggregation, indicate that future designs that incorporate both polar and apolar residues within the cavity should have little difficulty with protein assembly or stability. As demonstrated herein, the versatile ferritin scaffold will make it possible to engineer proteins with new nanoscale functions.

Acknowledgment. I.J.D. thanks the ACS Petroleum Research Fund, a Camille and Henry Dreyfus New Faculty Award, and the NSF (DMR 0520020) for support of this work. J.G.S. acknowledges support from NIH (GM-61267) and the NSF (CHE 9984752 and DMR 0079909, 0520020, and 0425780). We thank Feng Gai (UPenn) for use of a CD spectrometer and fluorometer, Roberto Kolter (Harvard Medical School) for the cloned DpsWT construct, the UPenn Institute for Medicine and Engineering for access to DLS, and Vijay Yerubandi for experimental assistance. All Dps structural figures were made using PyMOL.[74] We remember Peter Snow at Caltech and thank him for his help in the initial protein expression.

Supporting Information Available: Analysis of Dps equilibrium unfolding studies and UV−vis spectra of iron-loaded proteins. This material is available free of charge via the Internet at http://pubs.acs.org.

JA057069X

(94) Santambrogio, P.; Levi, S.; Cozzi, A.; Rovida, E.; Albertini, A.; Arosio, P. *J. Biol. Chem.* **1993**, *268*, 12744−12748.